ACS Partner Journal

Journal of the American Society for Mass Spectrometry

pubs.acs.org/jasms

Research Article

Ground and Excited States of Gas-Phase DNA Nucleobase Cation-Radicals. A UV−vis Photodissociation Action Spectroscopy and Computational Study of Adenine and 9-Methyladenine

Shu R. Huang, Andy Dang, and František Tureček*

Cite This: *J. Am. Soc. Mass Spectrom.* 2020, 31, 1271−1281

Read Online

ACCESS | Metrics & More | Article Recommendations | Supporting Information

ABSTRACT: Cation radicals of adenine ($A^{\bullet+}$) and 9-methyladenine ($MA^{\bullet+}$) were generated in the gas phase by collision-induced intramolecular electron transfer in copper−terpyridine−nucleobase ternary complexes and characterized by collision-induced dissociation (CID) mass spectra and UV−vis photodissociation action spectroscopy in the 210−700 nm wavelength region. The action spectra of both $A^{\bullet+}$ and $MA^{\bullet+}$ displayed characteristic absorption bands in the near-UV and visible regions. Another tautomer of $A^{\bullet+}$ was generated as a minor product by multistep CID of protonated 9-(2-bromoethyl)adenine. Structure analysis by density functional theory and coupled-clusters ab initio calculations pointed to the canonical 9-H-tautomer **Ad1**$^{\bullet+}$ as the global energy minimum of adenine cation radicals. The canonical tautomer **MA1**$^{\bullet+}$ was also calculated to be a low-energy structure among methyladenine cation radicals. However, two new noncanonical tautomers were found to be energetically comparable to **MA1**$^{\bullet+}$. Vibronic absorption spectra were calculated for several tautomers of $A^{\bullet+}$ and $MA^{\bullet+}$ and benchmarked on equation-of-motion coupled-clusters excited-state calculations. Analysis of the vibronic absorption spectra of $A^{\bullet+}$ tautomers pointed to the canonical tautomer **Ad1**$^{\bullet+}$ as providing the best match with the action spectrum. Likewise, the canonical tautomer **MA1**$^{\bullet+}$ was the unequivocal best match for the $MA^{\bullet+}$ ion generated in the gas phase. According to potential-energy mapping, **MA1**$^{\bullet+}$ was separated from energetically favorable noncanonical cation radicals by a high-energy barrier that was calculated to be above the dissociation threshold for loss of a methyl hydrogen atom, thus preventing isomerization. Structures and energetics of all four DNA nucleobase cation radicals are compared and discussed.

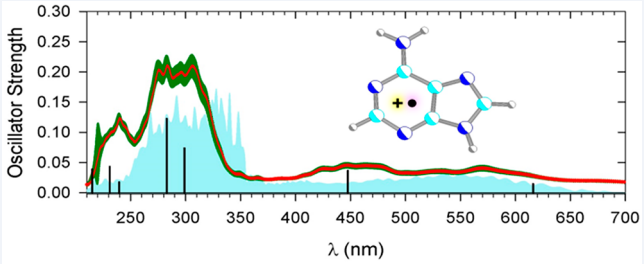

1. INTRODUCTION

Ionization of DNA by impact of high energy particles creates random electron vacancies in the nucleobases, forming transient cation radicals.[1] The chemical processes triggered by DNA ionization involve electron transfer and formation of radical intermediates that have been studied extensively with a focus on downstream reaction intermediates and products.[2−4] In contrast, the primary cation radicals have not been characterized spectroscopically so far because of fast proton transfer reactions with solvent and other species present in the condensed phase environment.[5] Isolated nucleobase cation radicals have been produced by electron ionization of gaseous nucleobases, and their unimolecular dissociations have been characterized by mass spectrometry.[6] Thus, the rarefied gas phase provides a suitable environment for the generation of nucleobase cation radicals and spectroscopic investigations of their structure and electronic properties. Several previous computational studies of nucleobase cation radicals have been chiefly focused on the determination of ionization energies and electron density distribution.[7−11] In addition to direct ionization, DNA nucleobase cation radicals have been generated by collision-induced intramolecular electron transfer and dissociation of ternary metal complexes formed by electrospray ionization (Scheme 1).[12] This method, that was originally introduced to generate peptide cation radicals,[13] has been adapted by O'Hair and co-workers to provide a useful technique for nucleobase cation-radical generation.[14,15] Combined with mass separation and ion trapping, the Scheme 1 reaction allowed for structure studies of the synthesized nucleobase cation-radicals using methods of photodissociation action spectroscopy.[16−18] Guanine,[19] 9-methylguanine,[19,20] 2′-deoxyguanosine,[21] and guanosine[19] have been characterized by infrared multiphoton photodissociation (IRMPD)[20] and UV−vis photodissociation (UVPD)[19] action spectroscopy. IRMPD and UVPD differ in the mode of resonant ion photoexcitation. IRMPD requires multiple infrared photons to deliver energy via vibrational excitation, resulting in slow heating of the ion at

Received: March 17, 2020
Revised: April 23, 2020
Accepted: April 23, 2020
Published: April 23, 2020

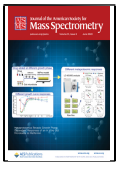

Scheme 1. Formation of Nucleobase Cation Radicals from Cu Complexes Showing M06-2X/6-31+G(d,p)-Optimized Geometries of Low Energy DNA Nucleobase Cation Radicals Generated Previously by This Technique[a]

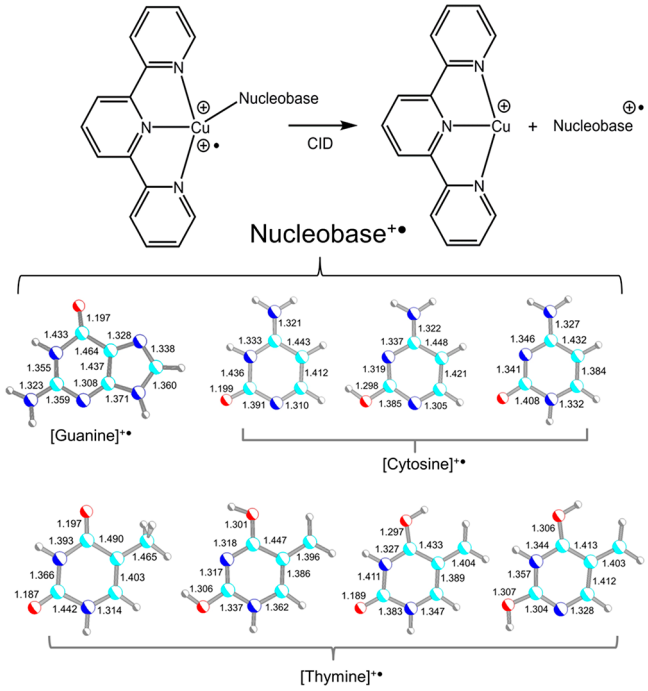

[a]Atom color coding is as follows: cyan = C, blue = N, red = O, gray = H. Bond lengths are in angstroms.

the resonant wavelength. In contrast, UVPD relies on single-photon electronic excitation whereby the absorbed energy either drives dissociation starting from an excited electronic state,[18] or provides vibrational excitation after internal conversion to the ground electronic state. Despite these differences, the IRMPD and UVPD results were in accord that the guanine-based cation radicals all had canonical nucleobase structures (Scheme 1).[19,20]

In contrast to guanine, IRMPD and UVPD action spectroscopy of cytosine cation radicals pointed to a mixture of tautomers (Scheme 1) formed by collision-induced intramolecular transfer and dissociation of ternary copper complexes.[22] This promiscuous behavior of cytosine cation radicals parallels neutral cytosine which is known to exist as multiple tautomers in the gas phase.[23−26] A recent study of the thymine cation radical has brought surprising results in that the major species generated from a copper complex were noncanonical tautomers (Scheme 1) that represented 77% of the tautomer mixture, as characterized by UVPD action spectroscopy and ion−molecule reactions.[27] All these spectroscopic studies have been corroborated by extensive ab initio calculations of equilibrium structures, energies, vibrational frequencies, and excited electronic states to characterize the gas-phase nucleobase cation radicals.

Here, we report the generation and UVPD spectroscopic study of adenine-based cation radicals. This completes the series of DNA nucleobase cation radicals and at the same time provides reference structural and spectroscopic data that may be used in studies of more complex cation radicals derived from nucleosides,[28] oligonucleotides,[29] and duplex DNA.

2. EXPERIMENTAL SECTION

Materials. Adenine, 9-methyladenine, copper nitrate, and 2:2′,6′:2″-terpyridine (terpy) were purchased from Sigma-Aldrich (St. Louis, MO) and used as received. 9-(2-Bromoethyl)adenine was purchased from Combi-Blocks (San Diego, CA). To prepare the [Cu(terpy)(adenine)] or [Cu(terpy)(9-methyladenine)] complexes, 0.011 mmol of adenine or 9-methyladenine was dissolved in 1 mL of 0.01 M $Cu(NO_3)_2$ and terpy in 5.25:1 acetonitrile−water. These stock solutions were diluted to 10 μM for infusion into the electrospray ion source.

Methods. Mass and photodissociation action spectra were measured on modified LTQ-XL ETD linear ion trap (Thermo Fisher, San Jose, CA) and amaZon Speed 3D ion trap tandem mass spectrometers (Bruker Daltonik, Bremen, Germany) equipped with an EKSPLA NL301G Nd:YAG laser (Altos Photonics, Bozeman, MT) working at 20 Hz frequency and 3 to 6 ns pulse width, as described previously.[30] The photon pulses were treated by a PG142C unit (Altos Photonics, Bozeman, MT), which incorporated a third harmonic generator and optical parametric oscillator coupled with an optional second harmonic generator to enable wavelength tuning in the range of 210−700 nm. The laser beam (6 mm diameter) exiting the PG142C unit was aligned and focused into the ion trap. The laser pulse energies were measured at each experimental wavelength using an EnergyMax-USB J-10MB energy sensor (Coherent Inc., Santa Clara, CA) to calibrate the action spectra. The measured photofragment ion intensities were normalized to the number of photons per pulse. The action spectra were reproduced and are reported as averages of two measurements performed on different days. The action spectra obtained on the LTQ and Bruker ion traps were comparable; the Bruker spectra are reported and discussed here, the LTQ spectra are given as Supporting Information (Figure S1). Accurate mass-to-charge ratios were obtained from high-resolution mass spectra that were measured on an Orbitrap Velos mass spectrometer (Thermo Fisher, San Jose, CA) at a resolving power of 60000.

Calculations. Ab initio and density functional theory (DFT) calculations were performed with the Gaussian 16 (Revision A03) suite of programs.[31] Structures were first optimized with B3LYP/6-31+G(d,p)[32] and CAM-B3LYP/6-311+G(2d,p)[33] to obtain a preliminary ranking of the cation-radical tautomers by energy and evaluate local energy minima by adequate harmonic frequencies. Additional sets of optimized geometries were obtained with Møller−Plesset[34] (MP2, full) and coupled-clusters[35] (single and double excitations, CCSD)[36] calculations with the 6-31+G(d,p) basis set, as well as with M06-2X[37] and the 6-31+G(d,p) and 6-311++G(2d,p) basis sets. All these calculations were performed within the spin-unrestricted formalism. Higher spin states in the UMP2 calculations were treated with the spin projection method[38,39] using spin annihilation that reduced the total spin close to the theoretical value (0.75). The purpose of the multiple geometry optimizations was to find the best match between the CCSD/6-31+G(d,p) optimized geometries on one hand, and the DFT and MP2(FULL) optimized geometries on the other. The match was established on the basis of total single-point energies calculated using coupled clusters with single, double, and disconnected triple excitations, CCSD(T),[36] that were extrapolated to the complete basis set (CBS),[40] providing benchmark relative energies. The extrap-

https://dx.doi.org/10.1021/jasms.0c00095
J. Am. Soc. Mass Spectrom. 2020, 31, 1271−1281

olation used an exponential formula reported recently,[19] the coefficients are summarized in Table S1 (Supporting Information). From these benchmarking calculations we established that CCSD(T)/CBS total energies based on M06-2X/6-31+G(d,p) and M06-2X/6-311++G(2d,p) geometries provided a close match with those based on CCSD/6-31+G(d,p) optimized geometries within 0.7 and 1.0 millihartree, respectively. Thus, geometry optimizations with M06-2X/6-31+G(d,p) can provide an inexpensive and highly accurate access to nucleobase structures that rival that of CCSD. Transitions and oscillator strength for 10 excited electronic states were evaluated using equation-of-motion CCSD (EOM-CCSD) calculations[41] with the 6-31+G(d,p) basis set. This covered excitations down to 220 nm for all tautomers. The EOM-CCSD transitions were used to benchmark the time-dependent DFT (TD-DFT)[42] calculations that were carried out with M06-2X for 35−40 excited states in adenine and 9-methyladenine cation radicals, covering the wavelength range to below 180 nm. The M06-2X TD-DFT calculations with the 6-31+G(d,p) and 6-311++G(2d,p) basis sets gave very similar results in terms of excitation energies that showed a close correlation: ΔE_{exc}[M06-2X/6-31+G(d,p)] = 1.0043 × ΔE_{exc}[M06-2X/6-311++G(2d,p)], r^2 = 0.9998, and a root-mean square deviation of rmsd = 0.024 eV for **Ad1**$^{\bullet+}$−**Ad679**$^{\bullet+}$ (Table S2, Supporting Information). Likewise, the oscillator strengths calculated with M06-2X and the two basis sets showed rmsd = 0.0051 (Table S3, Supporting Information). Hence, the M06-2X/6-31+G(d,p) TD-DFT calculations were used to calculate all vibronic spectra at 310 K. The B3LYP/6-31+G(d,p) normal modes were used to generate vibrational configurations with the Newton X program,[43] that were ordered according to their Boltzmann factors at 310 K. Three hundred lowest-energy configurations were selected and submitted to TD-DFT M06-2X/6-31+G-(d,p) calculations for 20 excited states to generate the vibronic spectra reported here.

3. RESULTS AND DISCUSSION

3.1. Cation-Radical Generation. Electrospray ionization of solutions containing Cu^{2+} ions, terpy, and the nucleobase formed the respective [Cu(terpy)(adenine)] and [Cu(terpy)-(9-methyladenine)] complexes as doubly charged ions at *m/z* 215.5 and 222.5 for ^{63}Cu, that were selected by mass and submitted to collision-induced dissociation (CID), yielding the respective [adenine]$^{\bullet+}$ (A$^{\bullet+}$, *m/z* 135) and [9-methyladenine]$^{\bullet+}$ (MA$^{\bullet+}$, *m/z* 149) cation radicals (Figure 1a,1b) together with the complementary Cu(terpy)$^+$ ions at *m/z* 296. The Cu-complex dissociations were clean and efficient, forming few side products and providing the nucleobase cation radicals in good yields. The A$^{\bullet+}$ and MA$^{\bullet+}$ ions were further investigated by CID-MS^3 (Figure 2a-2c). CID of A$^{\bullet+}$ led to loss of NH_2, HCN, CH_2N_2, and 2HCN (Figure 2a), which are standard dissociations also occurring upon electron ionization of adenine.[6] CID of MA$^{\bullet+}$ resulted in a dominant loss of a hydrogen atom and HCN (Figure 2b). CID of MA$^{\bullet+}$ labeled with deuterium in the ND_2 group showed a predominant loss of light hydrogen (Figure 2c, inset) and hydrogen migrations accompanying the elimination of HCN and DCN. The CID spectra further indicated the suitable fragment ions to be used in UVPD action spectra measurements.

In addition to the formation of cation radicals from the nucleobase metal complexes, we explored other methods

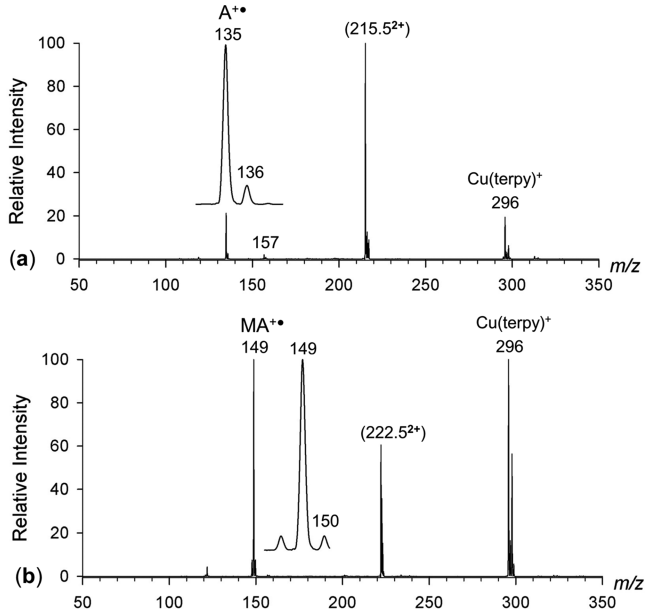

Figure 1. CID-MS^2 spectra of (a) [Cu(terpy)adenine]$^{2\bullet+}$ (*m/z* 215.5) and (b) [Cu(terpy)methyladenine]$^{2\bullet+}$ (*m/z* 222.5). Insets show the cation radical peak profiles.

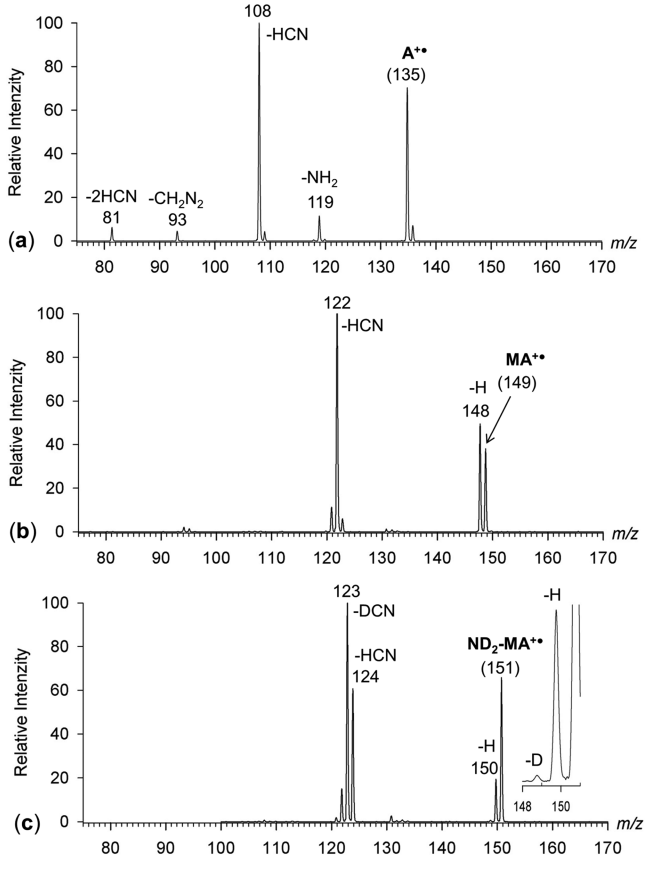

Figure 2. CID-MS^3 spectra of (a) [adenine]$^{\bullet+}$, (b) [9-methyladenine]$^{\bullet+}$, and (c) [ND_2-9-methyladenine]$^{\bullet+}$.

(Scheme 2). Bromination of 9-methyladenine at C-8 followed by electrospray ionization produced (MABr + H)$^+$ ions which upon CID underwent loss of Br forming *m/z* 149 ions corresponding to $C_6H_7N_5^{\bullet+}$ by high resolution MS. In another approach, protonation of 9-(2-bromoethyl)adenine yielded the

https://dx.doi.org/10.1021/jasms.0c00095
J. Am. Soc. Mass Spectrom. 2020, 31, 1271−1281

Scheme 2. Alternative Formation of Adenine Cation Radicals[a]

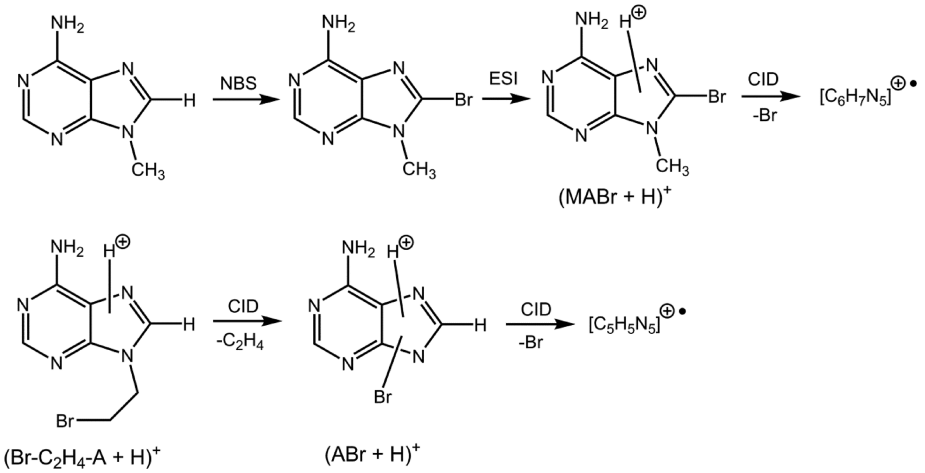

[a]NBS stands for bromination with *N*-bromosuccinimide in dichloromethane.

corresponding $(Br{-}C_2H_4{-}A + H)^+$ ion that upon CID-MS^2 eliminated C_2H_4, forming a bromoadenine ion, $(ABr + H)^+$, which afforded $C_5H_5N_5^{\bullet+}$ upon CID-MS^3. This fragment ion was characterized by its accurate mass (m/z 135.0525). The CID-MS^n spectra of thus generated $C_5H_5N_5^{\bullet+}$ and $C_6H_7N_5^{\bullet+}$ ions displayed the same fragment ions as the CID spectra of the respective $A^{\bullet+}$ and $MA^{\bullet+}$ that did not indicate any distinctive features.

3.2. UVPD Action Spectra. To characterize the adenine cation radicals and explore their electronic structure, we obtained UVPD action spectra in the valence-electron excitation region of 210−700 nm (5.90 to 1.77 eV excitation energy range). The action spectrum of $A^{\bullet+}$ (Figure 3a) showed several bands that were distinguished by mass-resolved photofragmentation channels. The bands with maxima at 580, 330, and 290 nm were represented by the major m/z 108 fragment by loss of HCN. The bands at 480, 340, 270, and 225 nm were due to the m/z 81 fragment ion (loss of 2 HCN), while the m/z 93 fragment ion formed bands at 280 and 320 nm. It is noteworthy that neutral adenine,[44−46] as well as the protonated ion[47,48] do not have absorption bands above 280 nm, and thus the major bands in the action spectrum of $A^{\bullet+}$ are due to electron transitions in the radical chromophore.

The action spectrum of the $C_5H_5N_5^{\bullet+}$ ion from 9-(2-bromoethyl)adenine showed similar bands although at different photofragmentation intensities (Figure 3b). The main differences were in the diminished intensity of the 580 and 480 nm bands carried by the m/z 108 and 81 fragment ions and substantially increased intensities of the 300, 280, and 220 nm bands (Figure 3b). This indicated that the $C_5H_5N_5^{\bullet+}$ ion in question could be a mixture of tautomers. Subtraction of the normalized Figure 3a,b spectra furnished the difference spectrum (Figure 3c) which chiefly displayed bands in the 220−300 nm region.

Turning to $MA^{\bullet+}$, the action spectrum displayed overlapping bands of the m/z 148 (loss of H) and m/z 122 (loss of HCN) fragment ions giving rise to a maximum at 580 nm (Figure 4). Further absorption bands carried by these two major channels were found at 340, 320, 270, and 215 nm. Again, the major absorption bands at $\lambda > 300$ nm were associated with electron excitations in the cation-radical chromophore.

We attempted to generate isomeric $C_6H_7N_5^{\bullet+}$ ions by CID bromine loss from protonated bromomethyladenine (Scheme 2). However, the action spectrum of this $C_6H_7N_5^{\bullet+}$ ion (Figure S2, Supporting Information) was superimposable with that of $MA^{\bullet+}$ across the entire wavelength region, indicating that these ions were identical.

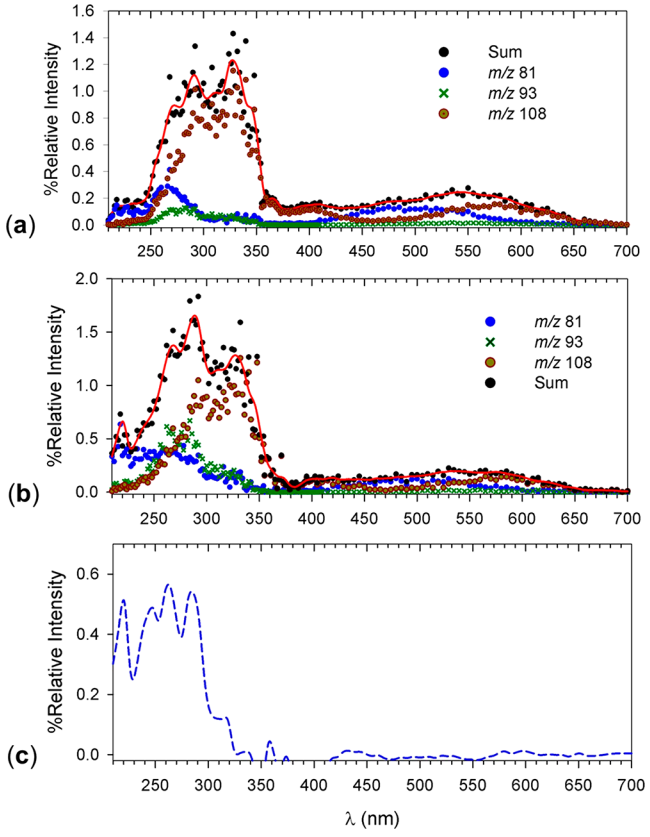

Figure 3. Action spectra of (a) $[adenine]^{\bullet+}$ and (b) m/z 135 ion from 9-(2-bromoethyl)adenine. (c) Difference spectrum of (a) and (b).

3.3. Adenine Ion Structures and Spectra Assignment. To assign the action spectra of adenine cation radicals, we used DFT and ab initio geometry optimizations to generate a number of $C_5H_5N_5^{\bullet+}$ tautomers (Figure 5) that were ranked by energy. Table 1 summarizes the 0 K relative energies obtained by the M06-2X and CCSD(T) calculations. Relative energies obtained by the other DFT and ab initio methods are

https://dx.doi.org/10.1021/jasms.0c00095
J. Am. Soc. Mass Spectrom. 2020, 31, 1271−1281

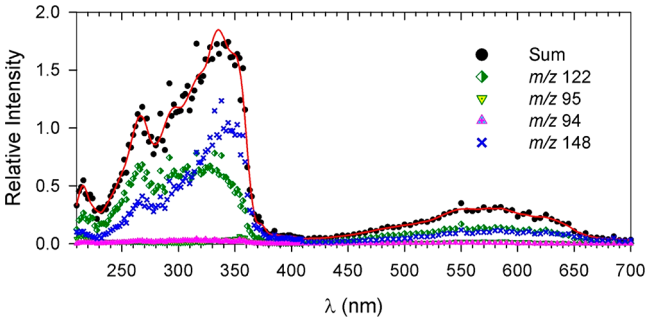

Figure 4. Action spectrum of [9-methyladenine]$^{\bullet+}$.

given in Table S4. The canonical N-9-H tautomer **Ad1**$^{\bullet+}$ was the lowest energy tautomer among adenine cation radicals.[8] This followed the ranking of neutral adenine molecules in the gas phase, where the canonical form **Ad1n** is also the lowest energy tautomer (Figure S3, Table S5)[49] and prevails in the gas phase.[50] The CCSD(T)/CBS-calculated adiabatic ionization energy of **Ad1n**, IE_{adiab} = 8.32 eV, which was based on CCSD/6-31+G(d,p)-optimized geometries (Table S6), was in an agreement with previously calculated values (8.18−8.33 eV)[7−11] and also with the experimental values from photoionization measurements (8.2−8.3 eV).[51] The other cation-radical tautomers, **Ad3**$^{\bullet+}$−**Ad88**$^{\bullet+}$, that differed in the distribution of the five hydrogen atoms on the purine skeleton, had significantly higher energies (Table 1). The tautomers are labeled to indicate the proton positions.

Vibronic spectra were calculated by M06-2X/6-31+G(d,p) TD-DFT for 20 lowest excited states, including excitations from 300 vibrational configurations of the cation radicals populated at 310 K. The calculated spectra of the four lowest-energy tautomers **Ad1**$^{\bullet+}$−**Ad7**$^{\bullet+}$ are shown in Figure 6, and the spectra of the other, higher energy, tautomes are shown in Figure S4. The excited-state assignments were based on benchmark EOM-CCSD calculations that were used to align the M06-2X data and assign the excited states (Tables S2 and S3, Supporting Information). Excited states of very low oscillator strength or those falling outside the experimental wavelength region are not annotated in Figure 6. The absorption spectrum of **Ad1**$^{\bullet+}$ (Figure 6a) showed bands of the ***B*** and ***D*** states that upon vibronic broadening provided the absorption features at 400−650 nm. This region covered the broad bands at 380−650 nm in the action spectrum of [adenine]$^{\bullet+}$ (Figure 3a). The most characteristic features of **Ad1**$^{\bullet+}$ were transitions to the ***F*** and ***G*** states that gave rise to the dual band in the absorption spectrum (Figure 6a). This provided a close match with the 330 and 290 nm bands in the action spectrum. The higher energy excitations at 239, 231, and 215 nm merged into a band at 240 nm upon vibronic broadening (Figure 6a). This band was present in the action spectrum, although at a lower intensity.

The calculated absorption spectra of the other tautomers displayed various degrees of mismatch with the action spectrum. For example, the spectrum of **Ad3**$^{\bullet+}$ did not show absorption above 550 nm, and lacked the band at 290 nm (Figure 6b). The spectrum of **Ad6**$^{\bullet+}$ had a different pattern of bands in the 210−350 nm region, namely, it displayed an intense band of the ***G*** state at 240 nm (Figure 6c) that did not have an equivalent in the action spectrum. Likewise, the

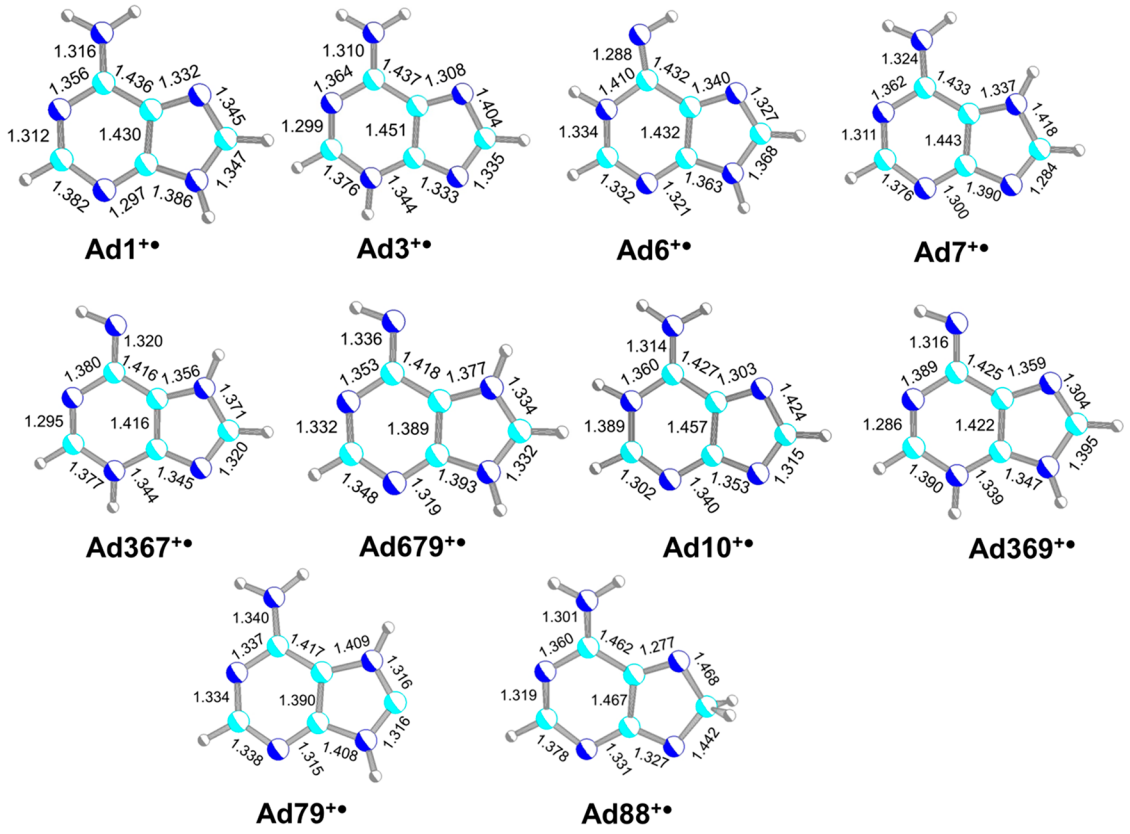

Figure 5. M06-2X/6-31+G(d,p)-optimized geometries of low-energy adenine cation radicals. Atom color coding as in Figure 1. Bond lengths are in angstroms.

https://dx.doi.org/10.1021/jasms.0c00095
J. Am. Soc. Mass Spectrom. 2020, 31, 1271−1281

Table 1. Adenine Cation-Radical Relative and Dissociation Energies

	relative energy[a,b]			
ion/reaction	M06-2X/6-31+G(d,p)	M06-2X/6-311++G(2d,p)	CCSD(T)/aug-cc-pVTZ[c]	CCSD(T)/CBS[d]
Ad1$^{\bullet+}$	0	0	0	0
Ad3$^{\bullet+}$	25	24	17	18
Ad6$^{\bullet+}$	21	21	22	22
Ad7$^{\bullet+}$	56	53	46	45
Ad367$^{\bullet+}$	42	43	45	46
Ad679$^{\bullet+}$	53	56	61	67
Ad10$^{\bullet+}$	68	66	66	58
Ad369$^{\bullet+}$	86	86	101	103
Ad79$^{\bullet+}$	130	133	132	-
Ad88$^{\bullet+}$	215	213	234	-
Ad1$^{\bullet+}$ → **F1**$^{\bullet+}$ + HCN	260	248	226	231
Ad1$^{\bullet+}$ → **F2**$^{\bullet+}$ + HCN	373	366	343	348

[a]In kJ mol^{-1}. [b]Including B3LYP/6-31+G(d,p) zero-point energies scaled with 0.975 and referring to 0 K in the gas phase. [c]Extrapolated to this basis set according to the linear formula: E[CCSD(T)/aug-cc-pVTZ] ≙ E[CCSD(T)/aug-cc-pVDZ] + E[MP2/aug-cc-pVTZ] − E[MP2/aug-cc-pVDZ]. [d]Single-point energies on CCSD/6-31+G(d,p) optimized geometries, extrapolated to the complete basis set; see Supporting Table S1.

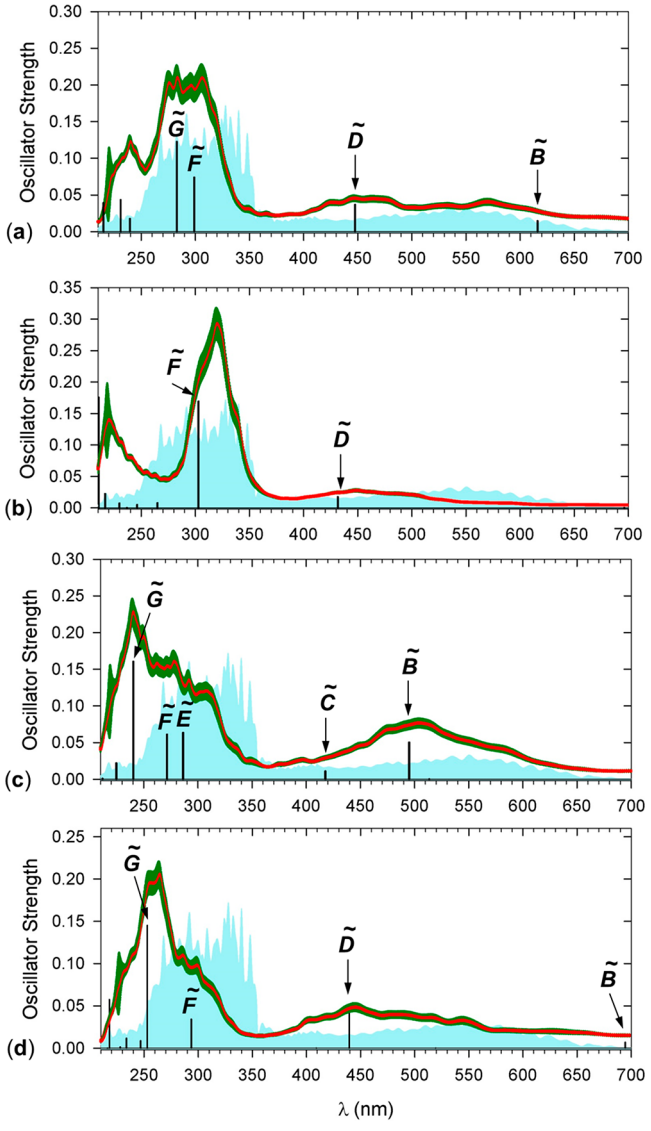

Figure 6. M06-2X/6-31+G(d,p) TD-DFT vibronic absorption spectra of (a) **Ad1**$^{\bullet+}$, (b) **Ad3**$^{\bullet+}$, (c) **Ad6**$^{\bullet+}$, and (d) **Ad7**$^{\bullet+}$. The blue shaded areas display the action spectrum presented as a sum of photofragment ion intensities and scaled for visual perusal.

absorption spectrum of **Ad7**$^{\bullet+}$ had prominent bands at 439 and 253 nm for the respective ***D*** and ***G*** excited states (Figure 6d) that did not match experimental bands in the action spectrum. Similar conclusions can be made for the absorption spectra of the higher-energy tautomers **Ad367**$^{\bullet+}$, **Ad679**$^{\bullet+}$, and **Ad10**$^{\bullet+}$ (Figure S4a−c) that did not match the action spectrum. Based on the vibronic spectrum and relative energy, we assign the gas-phase [adenine]$^{\bullet+}$ ion structure **Ad1**$^{\bullet+}$.

The component in the $C_5H_5N_5^{\bullet+}$ ion population formed from 9-(2-bromoethyl)adenine that was characterized by the difference action spectrum showed no bands above 330 nm (Figure 3c). This was best matched by the vibronic spectrum of N-1−H tautomer **Ad10**$^{\bullet+}$ (Figure 5). Although the match in this case was affected by the poorer quality of the difference spectrum, the band patterns in the 210−320 nm region were similar for the spectra of $C_5H_5N_5^{\bullet+}$ and **Ad10**$^{\bullet+}$ while quite dissimilar for the other tautomers.

3.4. 9-Methyladenine Ion Structures and Spectra Assignment. The presence of the 9-methyl group greatly reduced the number of cation-radical tautomers in this system (Figure 7). The canonical tautomer **MA1**$^{\bullet+}$ represented a low-energy structure followed by **MA6**$^{\bullet+}$ (Table 2). Other tautomers with an intact methyl group had substantially higher energies than **MA1**$^{\bullet+}$. However, additional, noncanonical, low-energy tautomers were generated in silico in which a methyl hydrogen atom was moved to N-1 (**MA91**$^{\bullet+}$), N-3 (**MA93**$^{\bullet+}$), or N-7 (**MA97**$^{\bullet+}$) (Table 2, Figure 7). The calculated vibronic spectrum of **MA1**$^{\bullet+}$ showed all of the features found in the action spectrum of MA$^{\bullet+}$. The broad band in the visible region of the action spectrum was represented by excitations to the ***B*** and ***C*** states of **MA1**$^{\bullet+}$ at 605 and 482 nm, respectively (Figure 8a). The two action spectrum bands with maxima at 340 and 270 nm were assigned to excitations to the ***F*** and ***G*** states at 293 and 274 nm, respectively. In contrast, the noncanonical MA tautomers were calculated to have no absorption maxima above 350−360 nm, while the most prominent bands were in the 200−250 nm region where the action spectrum showed only weak absorption (Figure 8b,8c). Based on the match of the vibronic spectrum and the low relative energy, the action spectrum was assigned to the canonical tautomer **MA1**$^{\bullet+}$.

3.5. Ion Dissociation Energies. The dissociative nature of the action spectra raised the question of the dissociation energetics of the lowest energy tautomers **Ad1**$^{\bullet+}$ and **MA1**$^{\bullet+}$.

https://dx.doi.org/10.1021/jasms.0c00095
J. Am. Soc. Mass Spectrom. 2020, 31, 1271−1281

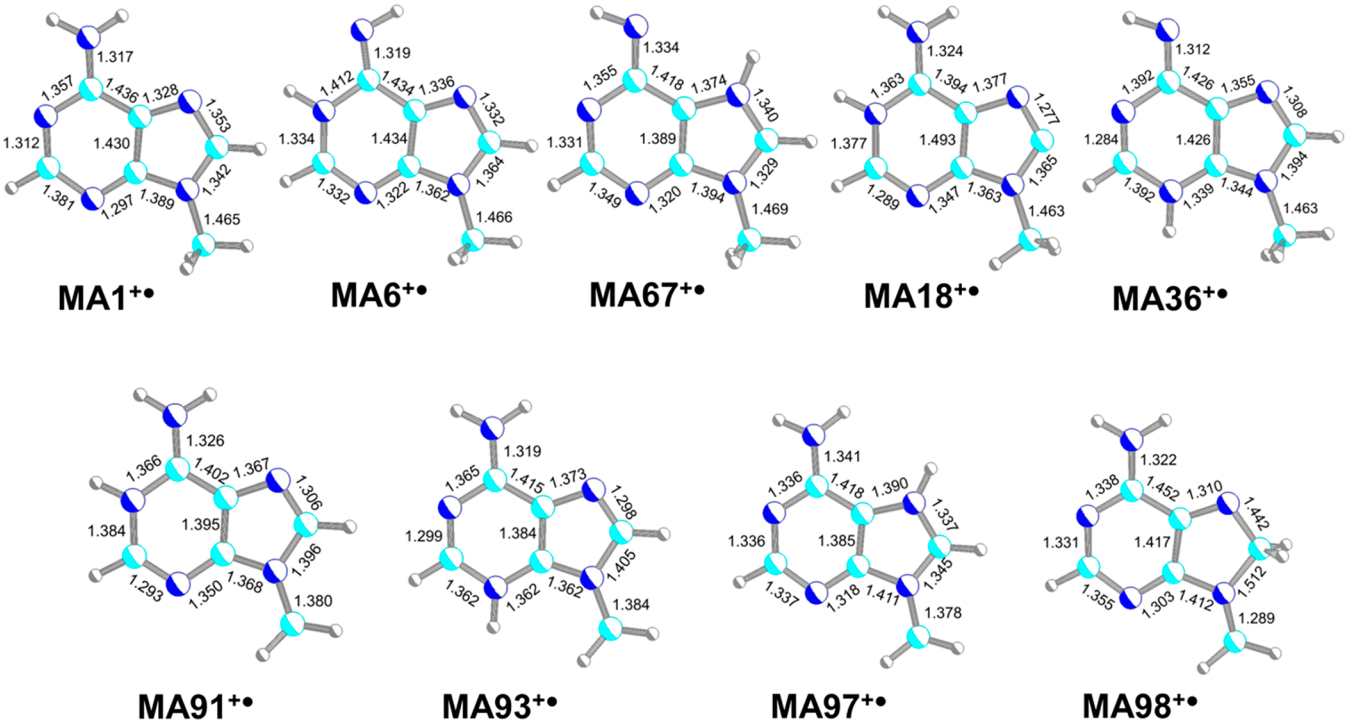

Figure 7. M06-2X/6-31+G(d,p)-optimized structures of low-energy $MA^{\bullet+}$ tautomers. Atom color coding as in Figure 1. Bond lengths are in angstroms.

Table 2. Relative and Dissociation Energies of Methyladenine Cation-Radicals

	relative energy[a,b]			
ion/reaction	M06-2X/ 6-31+G(d,p)	M06-2X/ 6-31+G(d,p)	CCSD(T)/ aug-cc-pVTZ[c]	CCSD(T)/ CBS[d]
MA1$^{\bullet+}$	0	0	0	0
MA6$^{\bullet+}$	23	23	19	22
MA67$^{\bullet+}$	49	52		
MA18$^{\bullet+}$	79	81	86	85
MA36$^{\bullet+}$	90	90		
MA91$^{\bullet+}$	−8	−6	−5	−8
MS93$^{\bullet+}$	4	4	5	2
MA97$^{\bullet+}$	22	24	25	23
MA98$^{\bullet+}$	82	81	83	87
MA1$^{\bullet+}$ → **MAf1**$^{+}$ + H	304	299	293	292
MA1$^{\bullet+}$ → TS(H-dis)	300	298	290	290

[a]In kJ mol^{-1}. [b]Including B3LYP/6-31+G(d,p) zero-point energies scaled with 0.975 and referring to 0 K in the gas phase. [c]Extrapolated to this basis set according to the linear formula: E[CCSD(T)/aug-cc-pVTZ] ≙ E[CCSD(T)/aug-cc-pVDZ] + E[MP2/aug-cc-pVTZ] − E[MP2/aug-cc-pVDZ]. [d]Single-point energies on CCSD/6-31+G-(d,p) optimized geometries, extrapolated to the complete basis set, see Supporting Table S1.

The most active dissociation channel of **Ad1**$^{\bullet+}$ by loss of hydrogen cyanide can in principle involve any of the [adenine]$^{\bullet+}$ nitrogen atoms and be associated with hydrogen atom migrations.[51−54] According to the analysis of threshold energies, formation of cation-radical fragment **Af1**$^{\bullet+}$ by loss of N-1 and C-2 required the lowest energy threshold at 231 kJ mol^{-1} (Table 1, Scheme 3). Other, isomeric, fragment ions (**Af2**$^{\bullet+}$, **Af3**$^{\bullet+}$, Scheme S1, Supporting Information) were calculated to have substantially higher energy thresholds (Table 1). Although the elimination of HCN may involve intermediates and transition states of above-threshold energies, it is worth noting that the lowest threshold energy is accessible by single-photon absorption at wavelengths of up to 520 nm. The fact that photodissociation is seen at wavelengths up to 650 nm (184 kJ mol^{-1} photon energy) can be explained by an extremely fast internal conversion of the ***B*** excited electronic state (Figure 3a,b) to the vibrationally excited ground state.[55−57] If the conversion occurs early in the laser pulse (3−6 ns), the ground state can absorb a second photon from the same pulse to drive dissociation. The most prominent dissociation of **MA1**$^{\bullet+}$ was a loss of a hydrogen atom. Out of several possible origins of the hydrogen atom we investigated, the loss of a methyl H was calculated to have the lowest threshold energy (292 kJ mol^{-1}, Table 1, Scheme 3). This can be delivered by a single photon with a wavelength of up to 424 nm. Again, the fact that photodissociation occurred with up to 650 nm photons indicated a sequential resonant absorption of two photons at these longer wavelengths. The action spectrum of $MA^{\bullet+}$ further indicated that the **MA1**$^{\bullet+}$ tautomer formed by CID of the Cu(terpy) complex did not isomerize to the thermodynamically favored ions **MA91**$^{\bullet+}$ and **MA93**$^{\bullet+}$. We investigated the possibility of an isomerization by a hydrogen migration from the methyl group to the sterically accessible N-3.

The potential energy surface for the migration (Figure S5, Supporting Information) showed a broad saddle at a large C−H separation (2.7 Å) whereby the N3−H bond at 1.85 Å was not yet formed. The in-plane migration forced the CH_2 group to be twisted out of the adenine ring plane, thus impairing π-electron interaction. Hence, the unfavorable geometry for the H atom migration was likely to prevent isomerization and formation of energetically favored tautomers. Both the C−H separation and potential energy for the migration exceeded the threshold values for the simple H atom loss, where the C−H

https://dx.doi.org/10.1021/jasms.0c00095
J. Am. Soc. Mass Spectrom. 2020, 31, 1271−1281

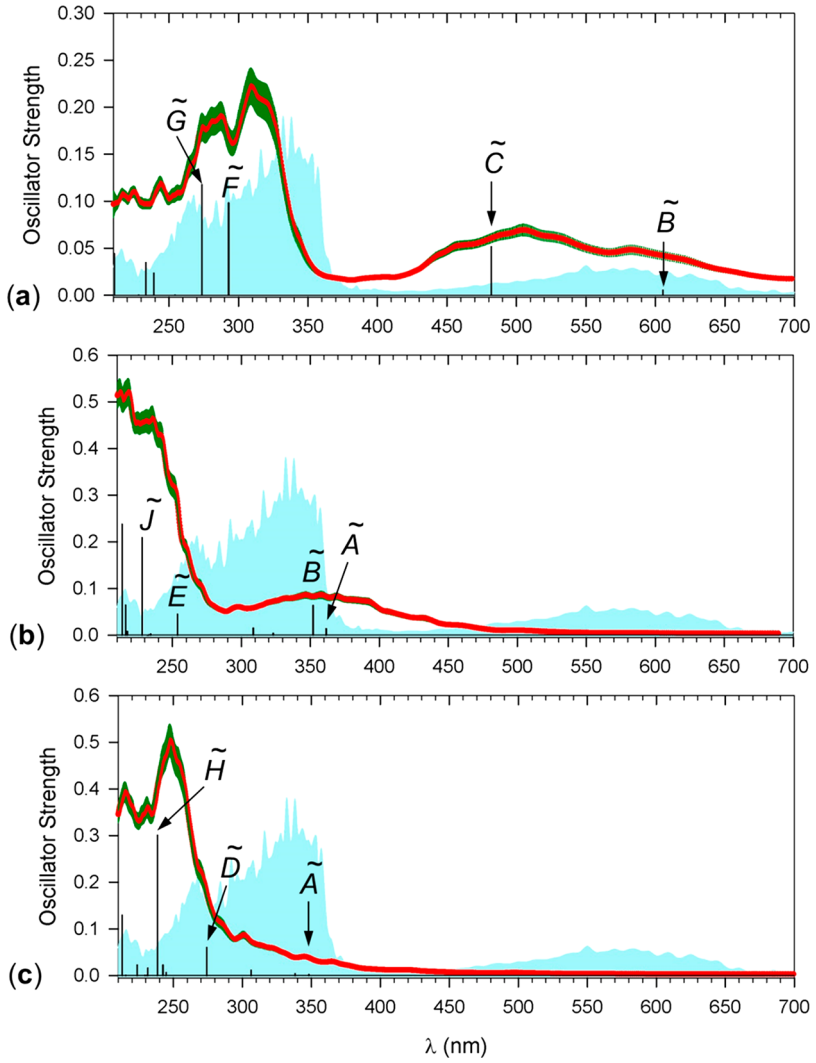

Figure 8. M06-2X/6-31+G(d,p) TD-DFT vibronic absorption spectra of (a) **MA1**$^{\bullet+}$, (b) **MA91**$^{\bullet+}$, and (c) **MA93**$^{\bullet+}$. The blue shaded areas are the action spectra presented as a sum of photofragment ion intensities and scaled for visual perusal.

Scheme 3. Major Dissociations of Ad1$^{\bullet+}$ **and MA1**$^{\bullet+}$

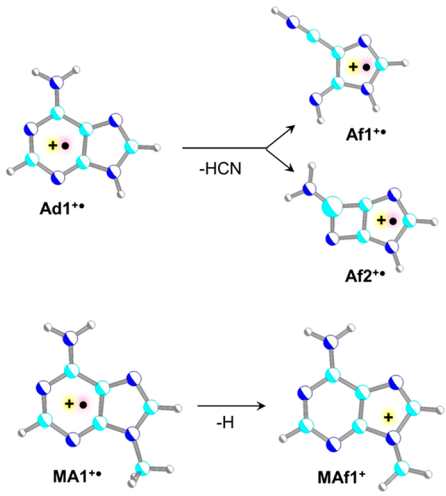

bond was essentially broken at 2.2 Å, and the H atom was departing at a 55° angle with respect to the adenine ring. This allowed the forming N=CH_2 group to become planar and conjugated with the adenine π-electron system.

3.6. Comparison of Adenine with the Other DNA Nucleobase Cation Radicals. The structure determination of the adenine and 9-methyladenine cation radicals as the respective canonical tautomers has completed the spectroscopic characterization of all four ionized DNA nucleobases. Energy calculations at the uniformly high level of theory indicate that the purine DNA nucleobases prefer the canonical forms. The stabilization of the canonical forms relative to the other tautomers, 14 and 2.8 kJ mol^{-1} for **Ad1**$^{\bullet+}$ and the guanine cation radical,[19] respectively, is relatively modest. The 9-methyl group has a mild effect on stabilizing tautomers of **MA1**$^{\bullet+}$ such as **MA91**$^{\bullet+}$, and the 6-OH tautomer of 9-methylguanine cation radical,[19] that are marginally more stable than the canonical forms. These global energy minima have not been yet observed experimentally and may require ingenious methods to be specifically generated in the gas phase. Importantly, however, UV−vis action spectra should provide unequivocal distinction of the isomeric adenine and guanine cation radicals, as evidenced by the current and previous studies.

Cation radicals derived from the pyrimidine nucleobases are more equivocal. The thymine cation radical has been shown to prefer noncanonical tautomers with OH groups produced by a

https://dx.doi.org/10.1021/jasms.0c00095
J. Am. Soc. Mass Spectrom. 2020, 31, 1271−1281

hydrogen migration from the 6-methyl.[27] This is in a sharp contrast with neutral thymine which exists as the lowest energy canonical dioxo form.[58] Based on their relative energies,[59] cytosine cation radicals also represent a substantial departure from the neutral nucleobase. Neutral cytosine tautomers have been calculated to prefer the *syn*- and *anti*-2-OH tautomers over the canonical 2-oxo-N-1-H form.[60] In contrast, among cytosine cation radical tautomers, the lowest energy belongs to the 2-oxo-N-3-H tautomer, followed by the *syn*- and *anti*-2-OH tautomers.[59] In accord with theory, an experimental study using infrared multiphoton and UV−vis action spectroscopies has identified a mixture of cytosine cation radical tautomers being produced in the gas phase.[22] An important point of the nucleobase cation-radical properties is whether or not they extend to a more complex DNA building blocs such as nucleosides and nucleotides. Previous studies of 2′-deoxyriboguanosine[21] and riboguanosine[19] have indicated that ionized guanine maintains the canonical structure in gas-phase nucleosides. The properties of the other DNA nucleoside cation radicals remain to be investigated.

4. CONCLUSIONS

Cation radicals of adenine and 9-methyladenine are formed as their low-energy canonical tautomers by collision-induced oxidation in ternary copper−terpy complexes. The structures have been corroborated by UV−vis action spectra and matching calculated vibronic spectra. New low-energy non-canonical tautomers of the 9-methyladenine cation radical have been identified computationally that present a challenge to experimental verification and spectroscopic characterization. Comparison of the populations and relative energies of DNA cation radicals points to the ionized purine nucleobases preferring canonical tautomer structures in the gas phase. In contrast, the ionized pyrimidine nucleobases are equivocal, forming mixtures of several tautomers in the gas phase. In order to apply these data to ionized DNA, the nucleobase cation-radical properties have to be extended by studies of more complex nucleosides and nucleotides. Computational studies to this end are in progress in this laboratory.

■ ASSOCIATED CONTENT

Supporting Information

The Supporting Information is available free of charge at https://pubs.acs.org/doi/10.1021/jasms.0c00095.

Figures of spectra and optimized structures, tables of CBS and excited state parameters (PDF)

■ AUTHOR INFORMATION

Corresponding Author

František Tureček − *Department of Chemistry, University of Washington, Seattle, Washington 98195-1700, United States;* orcid.org/0000-0001-7321-7858; Phone: +1-206-685-2041; Email: turecek@chem.washington.edu

Authors

Shu R. Huang − *Department of Chemistry, University of Washington, Seattle, Washington 98195-1700, United States*

Andy Dang − *Department of Chemistry, University of Washington, Seattle, Washington 98195-1700, United States*

Complete contact information is available at: https://pubs.acs.org/10.1021/jasms.0c00095

Notes

The authors declare no competing financial interest.

■ ACKNOWLEDGMENTS

Support of this research by the Chemistry Division of the U.S. National Science Foundation (Grant No. CHE-1661815) is gratefully acknowledged. F.T. thanks Klaus and Mary Ann Saegebarth Endowment for support.

■ REFERENCES

(1) Wagenknecht, H.-A., Ed. *Charge Transfer in DNA*; Wiley-VCH: Weinheim, Germany, 2005; pp 1−23.

(2) Schuster, G. B. Long-Range Charge Transfer in DNA: Transient Structural Distortions Control the Distance Dependence. *Acc. Chem. Res.* **2000**, *33*, 253−260.

(3) O'Neill, M. A.; Barton, J. K. Sequence-Dependent DNA Dynamics: The Regulator of DNA-Mediated Charge Transport. In *Charge Transfer in DNA*; Wagenknecht, H.-A., Ed.; Wiley-VCH: Weinheim, Germany, 2005; pp 27−31.

(4) Giese, B. Long-Distance Charge Transport in DNA: The Hopping Mechanism. *Acc. Chem. Res.* **2000**, *33*, 631−636.

(5) Steenken, S.; Jovanovic, S. V. How Easily Oxidizable Is DNA? One-Electron Reduction Potentials of Adenosine and Guanosine Radicals in Aqueous Solution. *J. Am. Chem. Soc.* **1997**, *119*, 617−618.

(6) NIST. *Chemistry WebBook*; Linstrom, P. J., Mallard, W. G., Eds.; NIST Standard Reference Database No. 69; National Institute of Standards and Technology: Gaithersburg, MD, 2019, http://webbook.nist.gov (retrieved July−December 2019).

(7) Sevilla, M. D.; Besler, B.; Colson, A. O. Ab Initio Molecular Orbital Calculations of DNA Radical Ions. 5. Scaling of Calculated Electron Affinities and Ionization Potentials to Experimental Values. *J. Phys. Chem.* **1995**, *99*, 1060−1063.

(8) Chen, X.; Syrstad, E. A.; Gerbaux, P.; Nguyen, M. T.; Tureček, F. Distonic Isomers and Tautomers of Adenine Cation Radical in the Gas Phase and Aqueous Solution. *J. Phys. Chem. A* **2004**, *108*, 9283−9293.

(9) Crespo-Hernandez, C. E.; Arce, R.; Ishikawa, Y.; Gorb, J.; Leszczynski, J.; Close, D. M. Ab Initio Ionization Energy Thresholds of DNA and RNA Bases in Gas Phase and in Aqueous Solution. *J. Phys. Chem. A* **2004**, *108*, 6373−6377.

(10) Cauet, E.; Dehareng, D.; Lievin, J. Ab Initio Study of the Ionization of the DNA Bases: Ionization Potentials and Excited States of the Cations. *J. Phys. Chem. A* **2006**, *110*, 9200−9211.

(11) Cauet, E.; Lievin, J. Radical Cations of the Nucleic Acid Bases and Radiation Damage to DNA: Ab initio Study. *Adv. Quantum Chem.* **2007**, *52*, 121−147.

(12) Gatlin, C. L.; Tureček, F.; Vaisar, T. Gas-Phase Complexes of Amino Acids with Copper(II) and Diimine Ligands. Part II. Amino Acids with O, N and S Functional Groups in the Side-chain. *J. Mass Spectrom.* **1995**, *30*, 1617−1627.

(13) Chu, I. K.; Rodriquez, C. F.; Lau, T. C.; Hopkinson, A. C.; Siu, K. W. M. Molecular Radical Cations of Oligopeptides. *J. Phys. Chem. B* **2000**, *104*, 3393−3397.

(14) Wee, S.; O'Hair, R. A. J.; McFadyen, W. D. Can Radical Cations of the Constituents of Nucleic Acids Be Formed in the Gas Phase Using Ternary Transition Metal Complexes? *Rapid Commun. Mass Spectrom.* **2005**, *19*, 1797−1805.

(15) Lam, A. K.; Abrahams, B. F.; Grannas, M. J.; McFadyen, W. D.; O'Hair, R. A. J. Tuning the Gas Phase Redox Properties of Copper(II) Ternary Complexes of Terpyridines to Control the Formation of Nucleobase Radical Cations. *Dalton Trans.* **2006**, 5051−5061.

(16) Dunbar, R. C. Photodissociation of Trapped Ions. *Int. J. Mass Spectrom.* **2000**, *200*, 571−589.

(17) Antoine, R.; Dugourd, P. UV-Visible Activation of Biomolecular Ions. (Laser Photodissociation and Spectroscopy of Mass-Separated Biomolecular Ions). *Lect. Notes Chem.* **2013**, *83*, 93−116.

(18) Polfer, N. C., Dugourd, P., Eds. Laser Photodissociation and Spectroscopy of Mass Separated Biomolecular Ions. *Lecture Notes in Chemistry*; Springer: Cham, 2013; Vol. 83, pp 13−20.
(19) Dang, A.; Liu, Y.; Tureček, F. UV-Vis Action Spectroscopy of Guanine, 9-Methylguanine and 2′-Deoxyguanosine Cation Radicals in the Gas Phase. *J. Phys. Chem. A* **2019**, *123*, 3272−3284.
(20) Feketeová, L.; Khairallah, G. N.; Chan, B.; Steinmetz, V.; Maître, P.; Radom, L.; O'Hair, R. A. J. Gas-Phase Infrared Spectrum and Acidity of the Radical Cation of 9-Methylguanine. *Chem. Commun.* **2013**, *49*, 7343−7345.
(21) Feketeova, L.; Yuriev, E.; Orbell, J. D.; Khairallah, G. N.; O'Hair, R. A. J. Gas-Phase Formation and Reactions of Radical Cations of Guanosine, Deoxyguanosine and Their Homodimers and Heterodimers. *Int. J. Mass Spectrom.* **2011**, *304*, 74−82.
(22) Lesslie, M.; Lawler, J. T.; Dang, A.; Korn, J. A.; Bím, D.; Steinmetz, V.; Maitre, P.; Tureček, F.; Ryzhov, V. Cytosine Radical Cation: A Gas-Phase Study Combining IRMPD Spectroscopy, UVPD Spectroscopy, Ion−Molecule Reactions, and Theoretical Calculations. *ChemPhysChem* **2017**, *18*, 1293−1301.
(23) Brown, R. D.; Godfrey, P. D.; McNaughton, D.; Pierlot, A. P. Tautomers of Cytosine by Microwave Spectroscopy. *J. Am. Chem. Soc.* **1989**, *111*, 2308−2310.
(24) Dong, F.; Miller, R. E. Vibrational Transition Moment Angles in Isolated Biomolecules: A Structural Tool. *Science* **2002**, *298*, 1227−1230.
(25) Nir, E.; Müller, M.; Grace, L. I.; de Vries, M. S. REMPI Spectroscopy of Cytosine. *Chem. Phys. Lett.* **2002**, *355*, 59−64.
(26) Alonso, J. L.; Vaquero, V.; Pena, I.; Lopez, J. C.; Mata, S.; Caminati, W. All Five Forms of Cytosine Revealed in the Gas Phase. *Angew. Chem., Int. Ed.* **2013**, *52*, 2331−2334.
(27) Dang, A.; Nguyen, H. T. H.; Ruiz, H.; Piacentino, E.; Ryzhov, V.; Tureček, F. Experimental Evidence for Non-Canonical Thymine Cation Radicals in the Gas Phase. *J. Phys. Chem. B* **2018**, *122*, 86−97.
(28) Liu, Y.; Dang, A.; Urban, J.; Tureček, F. Charge-Tagged DNA Radicals I the Gas Phase Characterized by UV/Vis Photodisociation Action Spectroscopy. *Angew. Chem., Int. Ed.* **2020**, DOI: 10.1002/anie.201916493.
(29) Liu, Y.; Korn, J. A.; Dang, A.; Turecek, F. Hydrogen-Rich Cation Radicals of DNA Dinucleotides. Generation and Structure Elucidation by UV-Vis Action Spectroscopy. *J. Phys. Chem. B* **2018**, *122*, 9665−9680.
(30) Dang, A.; Korn, J. A.; Gladden, J.; Mozzone, B.; Tureček, F. UV-Vis Photodissociation Action Spectroscopy on Thermo LTQ-XL ETD and Bruker amaZon Ion Trap Mass Spectrometers: A Practical Guide. *J. Am. Soc. Mass Spectrom.* **2019**, *30*, 1558−1564.
(31) Frisch, M. J.; Trucks, G. W.; Schlegel, H. B.; Scuseria, G. E.; Robb, M. A.; Cheeseman, J. R.; Scalmani, G.; Barone, V.; Petersson, G. A.; Nakatsuji, H.; Li, X.; Caricato, M.; Marenich, A. V.; Bloino, J.; Janesko, B. G.; Gomperts, R.; Mennucci, B.; Hratchian, H. P.; Ortiz, J. V.; Izmaylov, A. F.; Sonnenberg, J. L.; Williams-Young, D.; Ding, F.; Lipparini, F.; Egidi, F.; Goings, J.; Peng, B.; Petrone, A.; Henderson, T.; Ranasinghe, D.; Zakrzewski, V. G.; Gao, J.; Rega, N.; Zheng, G.; Liang, W.; Hada, M.; Ehara, H.; Toyota, K.; Fukuda, R.; Hasegawa, J.; Ishida, M.; Nakajima, T.; Honda, Y.; Kitao, O.; Nakai, H.; Vreven, T.; Throssell, K.; Montgomery, J. A., Jr.; Peralta, J. E.; Ogliaro, F.; Bearpark, M. J.; Heyd, J. J.; Brothers, E. N.; Kudin, K. N.; Staroverov, V. N.; Keith, T. A.; Kobayashi, R.; Normand, J.; Raghavachari, K.; Rendell, A. P.; Burant, J. C.; Iyengar, S. S.; Tomasi, J.; Cossi, M.; Millam, J. M.; Klene, M.; Adamo, C.; Cammi, R.; Ochterski, J. W.; Martin, R. L.; Morokuma, K.; Farkas, O.; Foresman, J. B.; Fox, D. J. *Gaussian 16*, revision A03; Gaussian, Inc.: Wallingford, CT, 2016.
(32) Becke, A. D. New Mixing of Hartree-Fock and Local Density-Functional Theories. *J. Chem. Phys.* **1993**, *98*, 1372−1377.
(33) Yanai, T.; Tew, D. P.; Handy, N. C. A New Hybrid Exchange-Correlation Functional Using the Coulomb-Attenuating Method (CAM-B3LYP). *Chem. Phys. Lett.* **2004**, *393*, 51−57.
(34) Møller, C.; Plesset, M. S. A Note on an Approximation Treatment for Many Electron Systems. *Phys. Rev.* **1934**, *46*, 618−622.
(35) Čížek, J. On the Use of the Cluster Expansion and the Technique of Diagrams in Calculations of Correlation Effects in Atoms and Molecules. *Adv. Chem. Phys.* **2007**, *14*, 35−89.
(36) Purvis, G. D., III; Bartlett, R. J. A. Full Coupled-Cluster Singles and Doubles Model - the Inclusion of Disconnected Triples. *J. Chem. Phys.* **1982**, *76*, 1910−1918.
(37) Zhao, Y.; Truhlar, D. G. The M06 Suite of Density Functionals for Main Group Thermochemistry, Thermochemical Kinetics, Noncovalent Interactions, Excited States, and Transition Elements: Two New Functionals and Systematic Testing of Four M06-Class Functionals and 12 Other Functionals. *Theor. Chem. Acc.* **2008**, *120*, 215−241.
(38) Schlegel, H. B. Potential Energy Curves Using Unrestricted Møller-Plesset Perturbation Theory with Spin Annihilation. *J. Chem. Phys.* **1986**, *84*, 4530.
(39) Mayer, I. Spin-Projected UHF Method. IV. Comparison of Potential Curves Given by Different One-Electron Methods. *Adv. Quantum Chem.* **1980**, *12*, 189−262.
(40) Halkier, A.; Helgaker, T.; Jørgensen, P.; Klopper, W.; Koch, H.; Olsen, J.; Wilson, A. K. Basis Set Convergence in Correlated Calculations on Ne, N2, and H2O. *Chem. Phys. Lett.* **1998**, *286*, 243−252.
(41) Comeau, D. C.; Bartlett, R. J. The Equation-of-Motion Coupled-Cluster Method. Applications to Open- and Closed-Shell Reference States. *Chem. Phys. Lett.* **1993**, *207*, 414−423.
(42) Furche, F.; Ahlrichs, A. Adiabatic Time-Dependent Density Functional Methods for Excited State Properties. *J. Chem. Phys.* **2002**, *117*, 7433−7447.
(43) Barbatti, M.; Ruckenbauer, M.; Plasser, F.; Pittner, J.; Granucci, G.; Persico, M.; Lischka, H. Newton-X: A Surface-Hopping Program for Nonadiabatic Molecular Dynamics. *Wiley Interdisciplinary Reviews: Comput. Mol. Sci.* **2014**, *4*, 26−33.
(44) Broo, A.; Holmen, A. Calculations and Characterization of the Electronic Spectra of DNA Bases Based on ab Initio MP2 Geometries of Different Tautomeric Forms. *J. Phys. Chem. A* **1997**, *101*, 3589−3600.
(45) Clark, L. B.; Peschel, G. G.; Tinoco, I., Jr. Vapor Spectra and Heat of Vaporization of Some Purine and Pyrimidine Bases. *J. Phys. Chem.* **1965**, *69*, 3615−3618.
(46) Sapunar, M.; Domcke, W.; Doslic, N. UV Absorption Spectra of DNA Bases in the 350−190 nm Range: Assignment and State Specific Analysis of Solvation Effects. *Phys. Chem. Chem. Phys.* **2019**, *21*, 22782−22793.
(47) Marian, C.; Nolting, D.; Weinkauf, R. The Electronic Spectrum of Protonated Adenine: Theory and Experiment. *Phys. Chem. Chem. Phys.* **2005**, *7*, 3306−3316.
(48) Pedersen, S. O.; Stochkel, K.; Byskov, C. S.; Baggesen, L. M.; Nielsen, S. B. Gas-Phase Spectroscopy of Prootnated Adenine, Adenosine 5′-monophosphate and Monohydrated Ions. *Phys. Chem. Chem. Phys.* **2013**, *15*, 19748−19752.
(49) Hanus, M.; Kabelac, M.; Rejnek, J.; Ryjacek, F.; Hobza, P. Correlated ab Initio Study of Nucleic Acid Bases and Their Tautomers in the Gas Phase, in a Microhydrated Environment, and in Aqueous Solution. Part 3. Adenine. *J. Phys. Chem. B* **2004**, *108*, 2087−2097.
(50) Brown, R. D.; Godfrey, P. D.; McNaughton, D.; Pierlot, A. P. A Study of the Major Gas-Phase Tautomer of Adenine by Microwave Spectroscopy. *Chem. Phys. Lett.* **1989**, *156*, 61−63.
(51) Orlov, V. M.; Smirnov, A. N.; Varshavsky, Ya. M. Ionization Potentials and Electron-Donor Ability of Nucleic Acid Bases and Their Analogs. *Tetrahedron Lett.* **1976**, *17*, 4377−4378.
(52) Bauer, C. Al.; Grimme, S. Elucidation of Electron Ionization Induced Fragmentations of Adenine by Semiempirical and Density Functional Molecular Dynamics. *J. Phys. Chem. A* **2014**, *118*, 11479−11484.
(53) Nelson, C. C.; McCloskey, J. A. Collison-Induced Dissociation of Adenine. *J. Am. Chem. Soc.* **1992**, *114*, 3661−3668.
(54) Dawley, M. M.; Tanzer, K.; Cantrell, W. A.; Plattner, P.; Brinkmann, N. R.; Scheier, P.; Denifl, S.; Ptasinska, S. Electron

https://dx.doi.org/10.1021/jasms.0c00095
J. Am. Soc. Mass Spectrom. 2020, 31, 1271−1281

Ionization of the Nucleobases Adenine and Hypoxanthine Near the Threshold: a Combined Experimental and Theoretical study. *Phys. Chem. Chem. Phys.* **2014**, *16*, 25039−25053.
(55) Luhrs, D. C.; Viallon, J.; Fischer, I. Excited-State Spectroscopy and Dynamics of Isolated Adenine and 9-Methyladenine. *Phys. Chem. Chem. Phys.* **2001**, 3, 1827−1831.
(56) Ullrich, S.; Schultz, T.; Zgierski, M. Z.; Stolow, A. Direct Observation of Electronic Relaxation Dynamics in Adenine via Time-Resolved Photoelectron Spectroscopy. *J. Am. Chem. Soc.* **2004**, *126*, 2262−2263.
(57) Kang, H.; Jung, B.; Kim, S. K. Mechanism for Ultrafast Internal Conversion of Adenine. *J. Chem. Phys.* **2003**, *118*, 6717−6719.
(58) Brown, R. D.; Godfrey, P. D.; McNaughton, D.; Pierlot, A. P. Microwave Spectrum of the Major Gas-Phase Tautomer of Thymine. *J. Chem. Soc., Chem. Commun.* **1989**, 37−38.
(59) Wolken, J. K.; Yao, C.; Tureček, F.; Polce, M. J.; Wesdemiotis, C. Cytosine Neutral Molecules and Cation-Radicals in the Gas-Phase. Structures, Energetics, Ion Chemistry, and Neutralization-Reionization Mass Spectrometry. *Int. J. Mass Spectrom.* **2007**, *267*, 30−42.
(60) Trygubenko, S. A.; Bogdan, T. V.; Rueda, M.; Orozco, M.; Lique, F. J.; Sponer, J.; Slavicek, P.; Hobza, P. Correlated ab Initio Study of Nucleic Acid Bases and Their Tautomers in the Gas Phase, in a Microhydrated Environment and in Aqueous Solution. Part 1. Cytosine. *Phys. Chem. Chem. Phys.* **2002**, *4*, 4192−4203.

https://dx.doi.org/10.1021/jasms.0c00095
J. Am. Soc. Mass Spectrom. 2020, 31, 1271−1281